Inorganic Chemistry

pubs.acs.org/IC
Article

Ferromagnetic Exchange and Slow Magnetic Relaxation in Cobalt Bis(1,2-dithiolene)-Bridged Dilanthanide Complexes

Alexandre H. Vincent, Daphné Lubert-Perquel, Stephen Hill, and Jeffrey R. Long*

Cite This: *Inorg. Chem.* 2024, 63, 24150−24156
Read Online

ACCESS | Metrics & More | Article Recommendations | Supporting Information

ABSTRACT: The construction of multinuclear lanthanide-based molecules with significant magnetic exchange interactions represents a key challenge in the realization of single-molecule magnets with high operating temperatures. Here, we report the synthesis and magnetic characterization of two series of heterobimetallic compounds, $(Cp^*_2Ln)_2(\mu\text{-}Co(pdt)_2)$ (Ln = Y^{3+}, Gd^{3+}, Dy^{3+}; pdt^{2-} = 1,2-diphenylethylenedithiolate) and $[K(18\text{-crown-6})][(Cp^*_2Ln)_2(\mu\text{-}Co(pdt)_2)]$ (Ln = Y^{3+}, Gd^{3+}), featuring two lanthanide centers bridged by a cobalt bis(1,2-dithiolene) complex. Dc magnetic susceptibility data collected for the Gd congeners indicate significant Gd−Co ferromagnetic exchange interactions with fits affording J = +11.5 and +7.33 cm^{-1}, respectively. Magnetization decay and ac magnetic susceptibility measurements carried out on the single-molecule magnet $(Cp^*_2Dy)_2(\mu\text{-}Co(pdt)_2)$ reveal full suppression of quantum tunneling and open-loop hysteresis persisting up to 3.5 K. These results, along with those of high-field EPR spectroscopy, suggest that transition metalloligands can enforce strong exchange interactions with adjacent lanthanide centers while maintaining a geometry that preserves molecular anisotropy. Furthermore, the magnetic properties of $[K(18\text{-crown-6})][(Cp^*_2Gd)_2(\mu\text{-}Co(pdt)_2)]$ show that increasing the spin of the ground state of the bridging complex may be a viable alternative to increasing J in obtaining well-isolated, strongly coupled magnetic ground states.

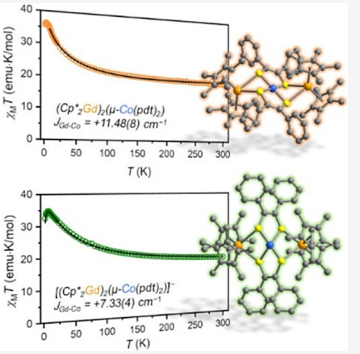

INTRODUCTION

Over the past three decades, single-molecule magnets have received significant attention from the chemistry and physics communities owing to their unique physical properties and their potential applications in devices for sensing, information storage, and data processing.[1−3] As a result of their large, unquenched orbital moments and magnetocrystalline anisotropies, the lanthanide ions have quickly outpaced transition metals in the design of single-molecule magnets exhibiting large relaxation barriers and high-temperature magnetic hysteresis.[4,5] However, unlike transition metals, the lanthanide ions typically exhibit vanishingly small magnetic exchange interactions in multinuclear clusters, due to the radially contracted nature of the valence 4f orbitals.[6]

The prospect of harnessing strong magnetic exchange in lanthanide-containing clusters to achieve large-moment, high-anisotropy ground states and eliminate the fast magnetic tunneling that plagues most lanthanide-only single-molecule magnets motivated early efforts to develop 3d−4f cluster single-molecule magnets.[7] However, magnetic exchange in these clusters is usually very weak (<1 cm^{-1}), and therefore slow magnetic relaxation of the exchange-coupled system typically occurs at very low temperatures, with single-ion relaxation dominating at higher temperatures. It was only with the discovery of the N_2^{3-} radical-bridged compounds $[\{[(Me_3Si)_2N]_2(THF)Ln\}_2(\mu\text{−}\eta^2\text{:}\eta^2\text{-}N_2)]^-$ (Ln = Gd, Tb, Dy)[8] that strong magnetic exchange was realized as a viable strategy for achieving high-performance single-molecule magnets with anisotropic Tb^{III} and Dy^{III} centers.[6,9] In these compounds, the diffuse nature of the N_2^{3-} radical spin orbital enables it to engage in direct exchange with unpaired electrons in the core-like lanthanide 4f orbitals.

Previous studies on transition metal-lanthanide exchange have centered on complexes featuring hard, unpolarizable bridging atoms that fail to produce any substantial exchange interactions due to their poor energy match and orbital overlap with the lanthanide 4f and 5d orbitals.[10,11] The recent synthesis and characterization of $[(Cp^*_2Ln)_2(\mu\text{-}MoS_4)]^-$ (Ln = Y, Gd, Tb, Dy),[12] each featuring an $S = {}^1/_2$ tetrathiomolybdate bridging unit, however, has demonstrated that metalloligands can support exchange interactions of similar magnitude to those observed for organic radical systems when softer, polarizable donor atoms like sulfur are employed.[12]

While $[(Cp^*_2Gd)_2(\mu\text{-}MoS_4)]^-$ exhibits strong ferromagnetic exchange, it was found that the Tb^{3+} and Dy^{3+} structural analogues only display weak butterfly hysteresis.[12] We posited this to be a consequence of the bridge geometry, as the

Received: September 9, 2024
Revised: November 19, 2024
Accepted: November 27, 2024
Published: December 9, 2024

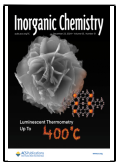

https://doi.org/10.1021/acs.inorgchem.4c03828
Inorg. Chem. 2024, 63, 24150−24156

Scheme 1. Synthetic Route to $(Cp^*_2Ln)_2(\mu\text{-}Co(pdt)_2)$ (1-Ln) (Ln = Y^{3+}, Gd^{3+}, Dy^{3+}) and $[K(18\text{-crown-6})][(Cp^*_2Ln)_2(\mu\text{-}Co(pdt)_2)]$ (2-Ln) (Ln = Y^{3+}, Gd^{3+})

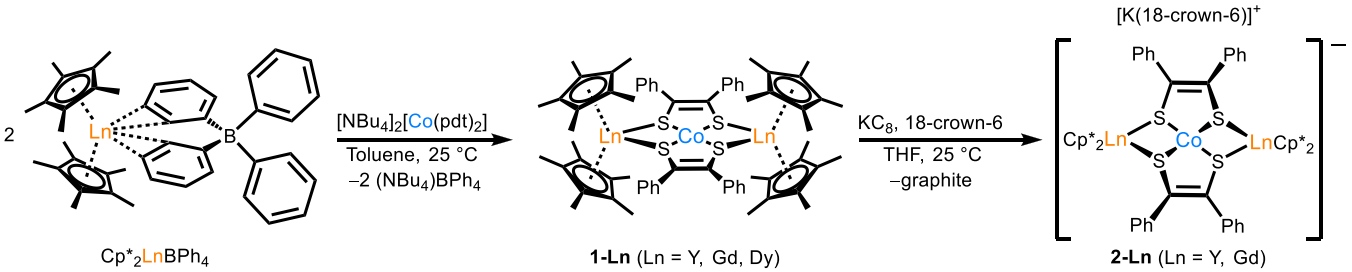

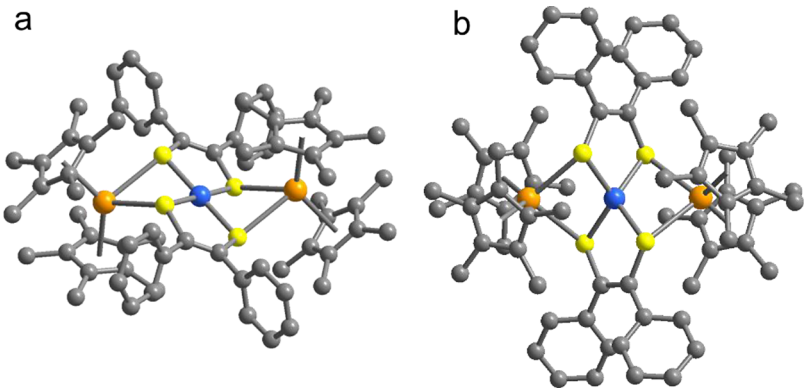

Figure 1. X-ray crystal structures for **1-Gd** (a) and **2-Gd** (b). Orange, blue, yellow, and gray spheres represent Gd, Co, S, and C, respectively; H atoms and an outer-sphere $[K(18\text{-crown-6})]^+$ ion for **2-Gd** have been omitted for clarity. The structure of **2-Gd** features two asymmetric units per unit cell, one with a C_2 axis through the metal-containing axis and one with a C_2 axis perpendicular to that axis. Selected interatomic distances (Å) and angles (°) for **1-Gd** and **2-Gd**. **1-Gd**; Gd–S 2.8320(6) and 2.8507(7) Å, Co–S 2.1771(6) and 2.1768(5) Å, Gd···Co 3.5176(4) Å, Gd–S–Co 88.20(2)° and 87.73(2)°, S–Gd–S 66.15(2), S–Co–S 90.85(2). **2-Gd**; Gd–S 2.793(1) and 2.803(1) Å, Co–S 2.235(1) and 2.237(1) Å, Gd···Co 3.1466(3) Å, Gd–S–Co 76.45(3)° and 76.35(3)°, S–Gd–S 87.37(3), S–Co–S 119.82(4).

tetrahedral metalloligand forced the quantization axes of each lanthanide ion into an orthogonal arrangement, preventing the formation of an anisotropic coupled ground state. Therefore, we began to consider alternative metalloligands with a square-planar geometry, similar to previously reported Cu–Gd heterobimetallic clusters.[13] We hypothesized that a ditopic square-planar bridge would enforce a parallel arrangement of the quantization axes for bound $[LnCp^*_2]^+$ subunits, thereby preserving anisotropy in the coupled ground state.

Herein, we show that the square-planar, $S = {}^1/_2$ cobalt dithiolene anion $[Co(pdt)_2]^{2-}$ (pdt^{2-} = 1,2-diphenylethylenedithiolate) can indeed bridge two $[LnCp^*_2]^+$ fragments, and that such a geometry results in open-loop magnetic hysteresis. Additionally, through a one-electron reduction, we are able to access a hitherto unobserved pseudotetrahedral $S = 1$ $[Co(pdt)_2]^{3-}$ bridging species, with a bridging configuration reminiscent of the $[\mu\text{-}Co(HAN)_2]^{5-}$ (HAN = hexaazatrinaphthylene) subunit in the recently reported $[K(Crypt)_6]\{Co^I[(\mu_3\text{-}HAN)M_2Cp^*_4]_2\}$ series of compounds (M = Gd or Dy).[14] This new trianionic bridge is presumably stabilized by the highly electrophilic environment between the two metallocenium cations. Both species exhibit appreciable ferromagnetic exchange interactions between the lanthanide centers and cobalt, with the strength of the exchange decreasing only slightly from $[Co(pdt)_2]^{2-}$ to $[Co(pdt)_2]^{3-}$.

RESULTS AND DISCUSSION

Synthesis and Structural Characterization. The $[Co(pdt)_2]^{2-}$-bridged complexes $(Cp^*_2Ln)_2(\mu\text{-}Co(pdt)_2)$ (**1-Ln**) were synthesized via salt metathesis between $Cp^*_2Ln(BPh_4)$ (Ln = Y, Gd, Dy) and $(NBu_4)_2[Co(pdt)_2]$ (Scheme 1). Slightly less than 0.5 equiv of $(NBu_4)_2[Co(pdt)_2]$ were used in the reactions to drive the formation of the desired dilanthanide compounds. Crystallization from layered benzene/HMDSO afforded red **1-Y**, **1-Gd**, and **1-Dy** as analytically pure crystalline solids. Single-crystal X-ray diffraction analysis of each **1-Ln** congener showed the compounds to be isostructural, with the lanthanide subunits related by a crystallographic inversion center at the central Co atom. Additionally, the bridging $[Co(pdt)_2]^{2-}$ unit retains the square-planar geometry of its unmetalated precursor $[NBu_4]_2[Co(pdt)_2]$ (Figure S6). As a result, the two lanthanide ions and four bridging sulfur atoms form a six-membered ring with a chairlike conformation (Figure 1a). The Co–S and alkene C–C distances are consistent with literature values for the $[Co(pdt)_2]^{2-}$ anion.[15] The Cp*(centroid)–Ln distances of **1-Ln** (see Table S3) lie within the range of values reported for structurally comparable compounds featuring $[MoS_4]^{2-}$ and PhS^- bridges (2.35–2.40 Å).[9,16−18] This result, together with the 2− charge state assignment for the bridging cobalt complex, suggests a negligible degree of charge transfer from the bridge to the lanthanide subunits.

Given the precedent for $S = 1$ $[Co(bdt)_2]^{1-}$ (bdt^{2-} = 1,2-benzenedithiolate),[19] we also targeted dinuclear compounds featuring the corresponding $[Co(pdt)_2]^-$ bridge. Cyclic voltammetry data collected for **1-Gd** (Figure S6) in 1,2-difluorobenzene revealed the first oxidation event to be irreversible, suggesting that **1-Gd** dissociates upon oxidation of the bridging $[Co(pdt)_2]^{2-}$ complex. A quasi-reversible

https://doi.org/10.1021/acs.inorgchem.4c03828
Inorg. Chem. 2024, 63, 24150−24156

feature at approximately −1.68 V vs $[Cp_2Fe]^{+/0}$, with a peak separation consistent with a one-electron process was observed, suggesting that the $[Co(pdt)_2]^{2-}$ subunit in **1-Gd** could unexpectedly undergo one-electron reduction. Indeed, the reaction of **1-Ln** (Ln = Y^{3+}, Gd^{3+}) with KC_8 in THF prompted an immediate color change from red to dark green, and following complexation with 18-crown-6, yielded the $[Co(pdt)_2]^{3-}$-bridged compounds $[K(18\text{-crown-6})]$-$[(Cp^*_2Ln)_2(\mu\text{-}Co(pdt)_2)]$ (**2-Ln**, Ln = Y, Gd). Crystallization from a THF solution layered with diethyl ether at room temperature resulted in the formation of dark green single crystals of **2-Y** and **2-Gd** in 22 and 42% yield, respectively.

We initially expected that the bridge in **2-Ln** would be isoelectronic and isostructural to known $S = 0$ d^8 square-planar nickel dithiolene complexes.[21] Indeed, $[Co(mnt)_2]^{3-}$ (mnt^{2-} = maleonitrile-2,3-dithiolate) was characterized as $S = 0$ based on the absence of an EPR signal in solution samples.[22] However, single-crystal X-ray diffraction analysis revealed that the bridging trianion in **2-Ln** adopts a pseudotetrahedral geometry with approximate D_{2d} symmetry (Figure 1b). We hypothesize that, rather than pairing with the electron in the singly occupied d_{xz}-derived molecular orbital in the parent compound, the added electron initially populates the highest σ antibonding orbital of $d_{x^2-y^2}$ character; reorganization to a tetrahedral geometry would then serve to minimize the antibonding character of the metal−ligand interactions. Regardless of the nature of the electron transfer, the geometric rearrangement about Co must be relatively facile in solution at ambient temperature, given the quasi-reversible profile of the cyclic voltammogram collected for **1-Gd**. The change in local geometry at Co in **1-Ln** is associated with a significant shortening of the lanthanide−cobalt distance by ∼0.37 Å. This shortening is accompanied by lengthening of the Gd−$Cp^*_{centroid}$ distances by ∼0.04 Å, indicating some degree of charge transfer from the bridge to each of the Cp^*_2Gd subunits (Table S4).

UV−Vis-NIR Diffuse Reflectance Spectroscopy. UV−vis-NIR diffuse reflectance spectra were collected for **1-Gd** and **2-Gd** to further investigate the nature of the bridging unit in each compound (Figure 2). The spectrum obtained for **1-Gd** exhibits features at high frequency in the visible region. The two transitions of weak intensity at 11,570 and 15,564 cm^{-1} are consistent with Laporte-forbidden d−d transitions. The subsequent transitions at 18,324, 18,867, 22,054, and 25,420 cm^{-1} feature higher intensities, consistent with ligand-to-metal charge transfer (LMCT). These observations are consistent with the expected spectral profile of $[Co(pdt)_2]^{2-}$, which should consist of high-energy LMCT and weak d−d transitions.[23] In the spectrum for **2-Gd**, transitions associated with LMCT appear between 17,980 and 25,000 cm^{-1}, while d−d transitions between 13,103 and 15,720 cm^{-1} dramatically increase in intensity. We ascribe this increase to the removal of inversion symmetry at Co and the consequent relaxation of the Laporte selection rule.[24] Crucially, two features are also present in the NIR region of the spectrum for **2-Gd** at 5896 and 7220 cm^{-1}, consistent with metal-to-metal charge transfer transitions.[12]

EPR Spectroscopy. In view of the precedent for substantial g-factor anisotropy in square-planar low-spin cobalt compounds,[22,25] we collected high-field EPR spectra for a finely powdered sample of **1-Y** to obtain the g values unambiguously. With these values in hand, extracting the exchange constant J_{Gd-Co} from subsequent fitting of dc magnetic susceptibility data can be done with a much higher degree of confidence. Indeed, the variable-frequency EPR spectra of **1-Y** (Figure 3) show a dominant $S = {}^1/_2$ species with pronounced g factor anisotropy (g_x = 3.42, g_y = 3.03, g_z = 1.8). Moreover, the anisotropic hyperfine pattern (A_x = 620 MHz, $A_y = A_z = 0$) is consistent with D_{2h} square-planar cobalt(II),[26] accounting for 90% of the observed signal.

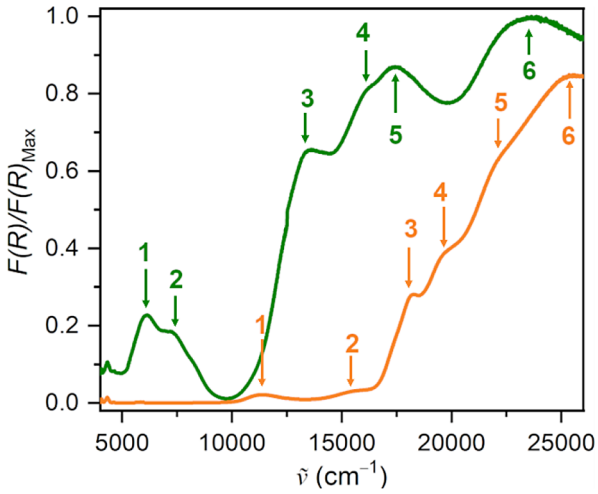

Figure 2. Diffuse reflectance spectra for **1-Gd** (orange trace) and **2-Gd** (green trace). The y-axis shows pseudoabsorbance (F(R)) normalized to the maximum observed peak height, where pseudoabsorbance is the Kubelka−Munk conversion of the raw diffuse reflectance spectrum.[20] Approximate peak locations are listed in wavenumbers in Table S6.

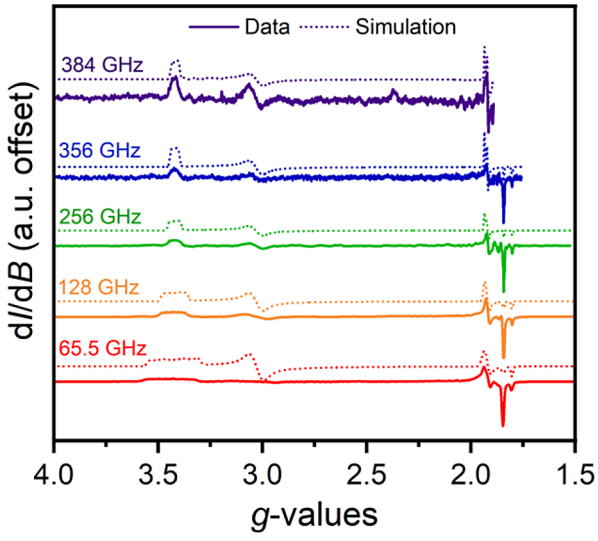

Figure 3. Continuous-wave variable-frequency, high-field EPR spectra for a solid-state powder sample of **1-Y**, shown in derivative mode. Each simulation corresponds to a linear combination of a dominant species α (90%) and minor species β (10%), as detailed in Figure S20.

Dc Magnetic Susceptibility Data. Variable-temperature dc magnetic susceptibility data were collected for **1-Ln** (Ln = Gd, Dy) and **2-Gd** from 2 to 300 K under an applied field of 0.1 T. The $\chi_M T$ product for **1-Gd** at 300 K is 19.5 emu K/mol, slightly greater than the 16.6 emu K/mol predicted for two noninteracting $S = {}^7/_2$ Gd^{3+} centers and an $S = {}^1/_2$ $[Co(pdt)_2]^{2-}$ complex with the g-values from the EPR analysis. With increasing temperature, $\chi_M T$ decreases monotonically,

https://doi.org/10.1021/acs.inorgchem.4c03828
Inorg. Chem. 2024, 63, 24150−24156

which is consistent with a ferromagnetic ground state with a large $\chi_M T$ value undergoing thermal depopulation with increasing temperature. The expected $\chi_M T$ value of the fully populated coupled ground state for **1-Gd** (two S = 7/2 Gd ions and one S = 1/2 Co ion with *g*-value anisotropy) is 33.5 emu·K/mol, which is close to the experimentally observed maximum value of 36.3 emu K/mol, when accounting for intermolecular ferromagnetic interactions. Accordingly, the magnetic data were fit in PHI[27] using a Heisenberg-exchange Hamiltonian (eq S1) to afford a coupling constant of J_{Gd-Co} = +11.48(8) cm^{-1}. The ferromagnetic nature of this interaction is in accord with those of other 3d−4f heterobimetallic systems. For instance, Gd−Cu compounds are known to exhibit ferromagnetic exchange interactions on the order of ∼2−3 cm^{-1} with little apparent electron transfer between the Cu and Gd ions.[28−30] The exchange interactions in these compounds are often ascribed to the strong configuration interaction between the charge-localized ground state and charge transfer excited states.[31] The notably greater exchange interaction strength observed in **1-Gd** vs typical 4f−3d compounds suggests that the sulfur bridging atoms improve the strength of this configuration interaction.[31]

At *T* = 300 K, dc magnetic susceptibility data obtained for **2-Gd** (Figure 4b) show $\chi_M T$ = 18.4 emu K/mol, slightly higher than the expected value for an uncoupled *S* = 1 Co^I center and two *S* = $^7/_2$ Gd^{3+} ions. The slightly larger $\chi_M T$ at 300 K over the expected uncoupled value and the monotonic rise in $\chi_M T$ with decreasing temperature is indicative of ferromagnetic coupling between the Gd and Co. The data were fit to a single-exchange Hamiltonian (eq S2), which yielded J_{Gd-Co} = +7.33(4) cm^{-1}.

Simultaneous fitting of reduced magnetization (Figure S16) and $\chi_M T$ data for **2-Gd** yielded zero-field splitting values of |*D*| = 60(1) cm^{-1} and *E*/*D* = 0.30(9) for the bridging $[Co(pdt)_2]^{3-}$ unit. These values are consistent with an *S* = 1 Co^I center with local D_{2d} symmetry. High-field EPR measurements were also carried out on **2-Y** to better quantify *D* and *E* parameters, but no signal could be resolved. This result confirms that the zero-field splitting is quite pronounced, as the expected signals would lie outside of the measurable field and frequency ranges. Indeed, assuming the zero-field splitting parameters from fitting reduced magnetization data are correct, the field required to observe an *S* = 1 resonance at the maximum frequency available of 512 GHz with |*D*| = 60 cm^{-1} was calculated to be ∼45 T, which is far greater than the maximum available field of the employed spectrometer.

Slow Magnetic Relaxation in 1-Dy. As an initial probe of slow magnetic relaxation in **1-Dy**, we collected variable-field magnetization data for a microcrystalline powder sample (Figure 5), which revealed open magnetic hysteresis loops to temperatures as high as 3.5 K and a coercive field of 0.6 T at 2 K. While $[\mu\text{-}MoS_4]^{3-}$ promotes stronger magnetic exchange than does $[\mu\text{-}Co(pdt)_2]^{2-}$, the magnetic hysteresis loops of $[(Cp^*_2Dy)_2(\mu\text{-}MoS_4)]^-$ feature only weak butterfly hysteresis at 2 K, where the remanent magnetization is zero at zero field. We ascribe this higher-temperature behavior in **1-Dy** to the geometry of the bridge. Specifically, due to the inversion center at the Co site, the local quantization axes of the coupled lanthanide ions are pinned parallel to one another (Figure S18). This effect maximizes the magnetic anisotropy of the exchange-coupled ground state. In contrast, in the structure of $[(Cp^*_2Dy)_2(\mu\text{-}MoS_4)]^-$, the local quantization axes of $[DyCp^*_2]^+$ subunits are positioned in an orthogonal orientation with respect to one another (Figure S17), yielding undesirable easy plane anisotropy within the coupled ground state.[32]

Magnetization decay experiments were also carried out on **1-Dy** in the temperature range 2−3 K to verify that temperature-independent relaxation is fully suppressed at low temperature. Indeed, fits to an exponential decay function (eq S3) showed that the relaxation times remain strongly temperature-dependent from 2−3 K (Figure S14), with the longest relaxation times being on the order of 10^4 s. Moreover, ac magnetic

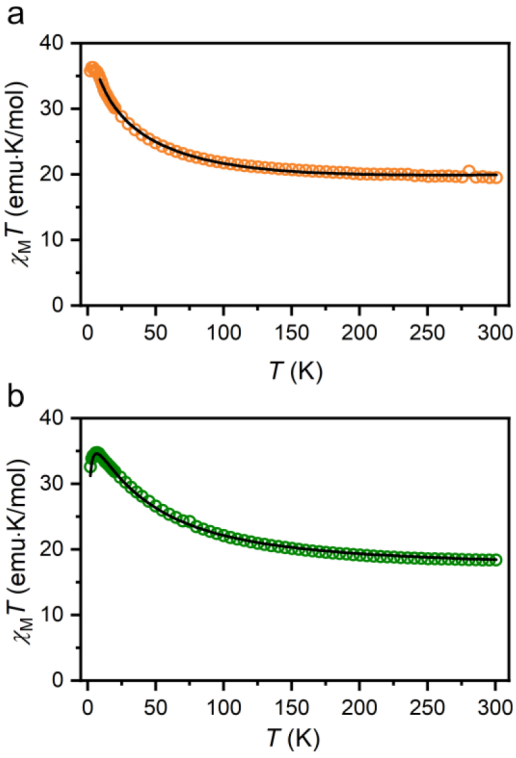

Figure 4. Variable-temperature dc magnetic susceptibility data for **1-Gd** (a) and **2-Gd** (b) under an applied field of 0.1 T. Black traces represent simulated curves using the following parameters: **1-Gd**: J_{Gd-Co} = +11.48(8) cm^{-1}, g_x = 3.42, g_y = 3.03, g_z = 1.8; **2-Gd**: J_{Gd-Co} = +7.33(4) cm^{-1}, |*D*| = 60(1) cm^{-1}, |*E*/*D*| = 0.30(9).

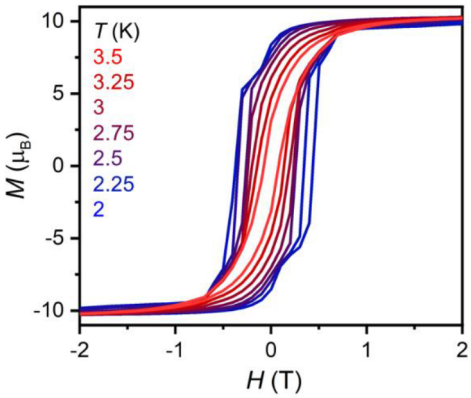

Figure 5. Magnetic hysteresis loops for **1-Dy** from 2−3.5 K in 0.25 K increments, with an average magnetic field sweep rate of 4.9 mT/s.

https://doi.org/10.1021/acs.inorgchem.4c03828
Inorg. Chem. 2024, 63, 24150−24156

susceptibility data collected under zero dc field and temperatures ranging from 6 to 20 K revealed a frequency-dependent signal in the out-of-phase susceptibility, χ_M'', with two clear, overlapping relaxation modes (Figure 6a). Given that the Dy ions are related by inversion symmetry, the presence of two distinct relaxation modes within the χ_M'' profile of **1-Dy** may indicate a wide dipolar field distribution within the sample.[34] These data were fit using the dual-process Debye model implemented in CCFIT2[33,35] to extract two sets of relaxation times (τ) at each temperature (Figure 6b). The faster of the two processes, denoted as process A, could be adequately fit to a Raman relaxation process (eq S4).[36] For the slower of the two relaxation processes (process B), the profile could be fit using an Orbach and Raman model (eq S5). Of note, temperature-independent relaxation is not evident at the ac or dc time scales measured here, suggesting that magnetic exchange in **1-Dy** mitigates tunneling of the magnetization of the type observed at low temperatures for $[(Cp^*_2Dy)_2(\mu\text{-}MoS_4)]^-$.[12]

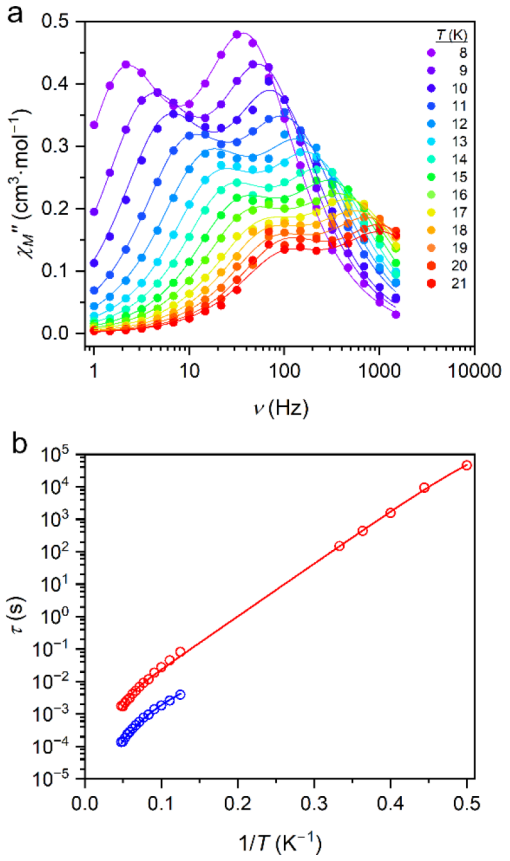

Figure 6. (a) Variable-frequency out-of-phase susceptibility (χ'') data for **1-Dy** at selected temperatures. Closed circles correspond to experimental data, and solid lines correspond to fits using the dual-mode generalized Debye model[33]; see Table S7 for fit parameters. (b) Arrhenius plot of relaxation time for **1-Dy**. Open circles in the range $\tau = 10^{-4}$–1 s correspond to average relaxation times derived from fits to ac susceptibility data using the dual-process Debye model, and open circles in the range $\tau = 10^2$–10^4 s were obtained from fits to isothermal zero-field magnetization decay in the range 2–3 K using an exponential decay function (Figure S13, eq S3). Blue and red circles correspond to relaxation processes A and B, respectively, as discussed in the text. Data corresponding to process A were fit in CCFIT2 using eq S4, while those corresponding to process B were fit in CCFIT2 using eq S5. Process A (blue) fit parameters: $C = 10^{-0.9(4)}$ s^{-1} K^{-n}, n = 3.6(3). Process B (red) fit parameters: U_{eff} = 26.05(4) cm^{-1}, $\tau_0 = 10^{-3.25(1)}$ s. $C = 10^{-7.37(2)}$ s^{-1} K^{-n}, n = 7.57(2).

CONCLUSIONS

The foregoing results detail the synthesis and characterization of **1-Ln** $(Cp^*_2Ln)_2(\mu\text{-}Co(pdt)_2)$ (Ln = Y, Gd, Dy) and **2-Ln** $[K(18\text{-crown-6})][(Cp^*_2Ln)_2(\mu\text{-}Co(pdt)_2)]$ (Ln = Y, Gd). A spectroscopic comparison between **1-Gd** and **2-Gd** was carried out to understand the differences in electronic structure between these species. In addition, the magnetic ground states and relaxation properties of **1-Gd**, **1-Dy**, and **2-Gd** have also been elucidated through SQUID magnetometry and through variable-frequency high-field EPR spectroscopic analysis of **1-Y**. The magnetic exchange coupling between Co and Gd in **1-Gd** is large and ferromagnetic, suggesting a double-exchange pathway. The magnetic exchange coefficient decreases upon reduction to **2-Gd**, however the bridge spin was found to increase to $S = 1$, increasing the exchange stabilization of the ferromagnetic ground state. These results demonstrate the utility of metalloligands in facilitating magnetic exchange between lanthanide ions, leading to suppression of zero-field tunneling and, consequently, open magnetic hysteresis loops persisting up to 3.5 K.

EXPERIMENTAL METHODS

Unless otherwise noted, all manipulations were performed under an atmosphere of dinitrogen or argon with rigorous exclusion of air and water using standard Schlenk and glovebox techniques. Tetrahydrofuran (THF), toluene, diethyl ether, and benzene were dried over alumina columns in a JC Meyer solvent system and were stored over 4 Å molecular sieves prior to use. Water and 1,4-dioxane were degassed by sparging with argon for 30 min immediately prior to use in the synthesis of $[Co(pdt)_2]_2$. Unless otherwise noted, other solvents used were degassed with three freeze pump thaw cycles and were dried over 4 Å molecular sieves for a minimum of 48 h prior to use. The precursor compounds $Cp^*_2LnBPh_4$ (Ln = Y, Gd, Tb, or Dy) were prepared as described previously.[16] Air-free elemental analyses were performed at the UC Berkeley Microanalytical facility. Proton NMR spectra were collected on a Bruker Avance AVB-400 MHz spectrometer at ambient temperature. Ultraviolet–visible-NIR diffuse reflectance spectra were collected on ground powders loosely packed on a bed of $BaSO_4$ under an N_2 atmosphere using a Varian Cary 5000 spectrometer. Infrared spectra were collected on neat samples using a Shimadzu IRSpirit FTIR spectrometer operating in attenuated total reflectance mode. Additional experimental details are included in Section 1 of the Supporting Information.

$(Cp^*_2Y)_2(\mu\text{-}Co(pdt)_2)$ (1-Y). Solid $Cp^*_2YBPh_4$ (271.3 mg, 0.3998 mmol) was suspended in toluene (15 mL) in a 20 mL scintillation vial. This suspension was quickly added with stirring to solid $[NBu_4]_2[Co(pdt)_2]$ (157.3 mg, 0.1529 mmol) in a separate 20 mL vial. Within seconds, the reaction mixture turned a red-orange color with concomitant formation of a colorless precipitate, presumed to be NBu_4BPh_4. The mixture was allowed to stir at ambient temperature for 12 h. The suspension was then centrifuged to separate the solids from solution and the toluene was decanted off into a separate vial. The toluene was then removed under vacuum to yield a dark red solid, which was dissolved with a minimal amount of benzene. The resulting red solution was filtered through diatomaceous earth, and hexamethyldisiloxane was slowly added to the resulting filtrate to precipitate a crystalline red-orange solid of analytical purity. Crystals suitable for single-crystal X-ray diffraction analysis were grown by layering concentrated solutions of benzene with hexamethyldisiloxane at room temperature. Yield: 83.4 mg, 43.3% based on $[NBu_4]_2[Co(pdt)_2]$. Calcd for $C_{68}H_{80}Y_2CoS_4$ (%): C, 64.7; H, 6.39. Found (%): C, 64.5; H, 6.35. ^{1}H NMR (400 MHz, benzene-d_6) δ 8.41 (s, 4H), 4.51 (s, 8H), 3.29 (s, 10H), 1.29 (s, 60H).

https://doi.org/10.1021/acs.inorgchem.4c03828
Inorg. Chem. 2024, 63, 24150–24156

$(Cp^*_2Gd)_2(\mu\text{-}Co(pdt)_2)$ (1-Gd). The compound was synthesized using a procedure analogous to that described for **1-Y**, using $Cp^*_2GdBPh_4$ (97.0 mg, 0.130 mmol) and $[NBu_4]_2[Co(pdt)_2]$ (51.1 mg, 0.0499 mmol). Yield: 24.4 mg, 35.1% based on $[NBu_4]_2[Co(pdt)_2]$ Calcd for $C_{68}H_{80}Gd_2CoS_4$ (%): C, 58.38; H, 5.76. Found (%): C, 57.24; H, 6.01.

$(Cp^*_2Dy)_2(\mu\text{-}Co(pdt)_2)$ (1-Dy). The compound was synthesized using a procedure analogous to that described for **1-Y**, using $Cp^*_2Dy(BPh_4)$ (147.3 mg, 0.1958 mmol) and $[NBu_4]_2[Co(pdt)_2]$ (76.6 mg, 0.0745 mmol). Yield: 45.0 mg, 42.8% based on $[NBu_4]_2[Co(pdt)_2]$. Calcd for $C_{68}H_{80}Dy_2CoS_4$ (%): C, 57.94; H, 5.72. Found (%): C, 57.81; H, 5.96.

[K(18-crown-6)][$(Cp^*_2Y)_2(\mu\text{-}Co(pdt)_2)$] (2-Y). Solid $(Cp^*_2Y)_2(\mu\text{-}Co(pdt)_2)$ (**1-Y**; 60.0 mg,0.0475 mmol) was dissolved in THF (5 mL). With stirring, 18-Crown-6 (14.9 mg, 0.0564 mmol) was added to the solution, followed by KC_8 (6.80 mg, 0.0504 mmol). Upon addition of KC_8, the solution changed from red-orange to a dark green color. The solution was then stirred at room temperature for 1 h to give a heterogeneous mixture. The mixture was centrifuged to separate the suspended graphite, and the THF solution was subsequently decanted. The THF was then removed under reduced pressure, leaving an oily dark green residue. The dark green residue was washed once with 5 mL of toluene to remove any unreacted starting material and excess 18-Crown-6. The resulting green solid was dissolved in a minimal amount of THF (∼1 mL), and the ensuing solution was then layered with diethyl ether and left to stand at room temperature. Block-shaped crystals suitable for single-crystal X-ray diffraction analysis formed after 24 h. Yield: 34 mg, 22% based on $(Cp^*_2Y)_2(\mu\text{-}Co(pdt)_2)$ Calcd for $C_{80}H_{104}CoKO_6S_4Y_2$ (%): C, 61.37; H, 6.70. Found (%): C, 60.88; H, 6.93.

[K(18-crown-6)][$(Cp^*_2Gd)_2(\mu\text{-}Co(pdt)_2)$] (2-Gd). The compound was synthesized using a procedure analogous to that described for **2-Y**, using **1-Gd** (49.6 mg, 0.0354 mmol), 18-Crown-6 (18.2 mg, 0.0689 mmol), and KC_8 (7.0 mg, 0.052 mmol). Yield: 25.4 mg, 42.1% based on $(Cp^*_2Gd)_2(\mu\text{-}Co(pdt)_2)$. Calcd for $C_{80}H_{104}CoKO_6S_4Gd_2$ (%): C, 56.44; H, 6.16. Found (%): C, 56.80 C; H, 6.44.

■ ASSOCIATED CONTENT

Supporting Information

The Supporting Information is available free of charge at https://pubs.acs.org/doi/10.1021/acs.inorgchem.4c03828.

Complete experimental methods, additional data, and cif files (PDF)

Accession Codes

Deposition Numbers 2329653−2329658 contain the supplementary crystallographic data for this paper. These data can be obtained free of charge via the joint Cambridge Crystallographic Data Centre (CCDC) and Fachinformationszentrum Karlsruhe Access Structures service.

■ AUTHOR INFORMATION

Corresponding Author

Jeffrey R. Long − *Department of Chemistry and Department of Chemical and Biomolecular Engineering, University of California, Berkeley, California 94720, United States; Materials Sciences Division, Lawrence Berkeley National Laboratory, Berkeley, California 94720, United States;* orcid.org/0000-0002-5324-1321; Email: jrlong@berkeley.edu

Authors

Alexandre H. Vincent − *Department of Chemistry, University of California, Berkeley, California 94720, United States;* orcid.org/0000-0002-9134-0435

Daphné Lubert-Perquel − *National High Magnetic Field Laboratory, Florida State University, Tallahassee, Florida 32310, United States; Department of Physics, University of Florida, Gainesville, Florida 32611, United States*

Stephen Hill − *National High Magnetic Field Laboratory, Florida State University, Tallahassee, Florida 32310, United States; Department of Physics and Department of Chemistry and Biochemistry, Florida State University, Tallahassee, Florida 32306, United States;* orcid.org/0000-0001-6742-3620

Complete contact information is available at: https://pubs.acs.org/10.1021/acs.inorgchem.4c03828

Author Contributions

The manuscript was written through contributions of all authors.

Notes

The authors declare no competing financial interest.

■ ACKNOWLEDGMENTS

This research was supported by NSF grant CHE-2102603. Resources of the Advanced Light Source, Beamline 12.2.1, a U.S. DOE Office of Science User Facility were utilized under contract no. DE-AC02-05CH11231. Support for the EPR experiments came from the Center for Molecular Magnetic Quantum Materials (M^2QM), an Energy Frontier Research Center funded by the U.S. Department of Energy, Office of Science, Basic Energy Sciences under Award DE-SC0019330. Work performed at the National High Magnetic Field Laboratory is supported by the NSF (DMR-1644779 and DMR-2128556) and the State of Florida. We thank Dr. T. David Harris for helpful discussions.

■ REFERENCES

(1) Atzori, M.; Sessoli, R. The Second Quantum Revolution: Role and Challenges of Molecular Chemistry. *J. Am. Chem. Soc.* **2019**, *141* (29), 11339−11352.

(2) Bogani, L.; Wernsdorfer, W. Molecular Spintronics Using Single-Molecule Magnets. *Nat. Mater.* **2008**, *7* (3), 179−186.

(3) Gatteschi, D.; Sessoli, R.; Villain, J. *Molecular Nanomagnets*; Oxford University Press, 2006.

(4) Goodwin, C. A. P.; Ortu, F.; Reta, D.; Chilton, N. F.; Mills, D. P. Molecular Magnetic Hysteresis at 60 K in Dysprosocenium. *Nature* **2017**, *548* (7668), 439−442.

(5) Woodruff, D. N.; Winpenny, R. E. P.; Layfield, R. A. Lanthanide Single-Molecule Magnets. *Chem. Rev.* **2013**, *113* (7), 5110−5148.

(6) Demir, S.; Jeon, I.-R.; Long, J. R.; Harris, T. D. Radical Ligand-Containing Single-Molecule Magnets. *Coord. Chem. Rev.* **2015**, *289*−*290*, 149−176.

(7) Liu, K.; Shi, W.; Cheng, P. Toward Heterometallic Single-Molecule Magnets: Synthetic Strategy, Structures and Properties of 3d−4f Discrete Complexes. *Coord. Chem. Rev.* **2015**, *289*−*290*, 74−122.

(8) Rinehart, J. D.; Fang, M.; Evans, W. J.; Long, J. R. Strong Exchange and Magnetic Blocking in N23−-Radical-Bridged Lanthanide Complexes. *Nat. Chem.* **2011**, *3* (7), 538−542.

(9) Demir, S.; Gonzalez, M. I.; Darago, L. E.; Evans, W. J.; Long, J. R. Giant Coercivity and High Magnetic Blocking Temperatures for N_2^{3-} Radical-Bridged Dilanthanide Complexes upon Ligand Dissociation. *Nat. Commun.* **2017**, *8* (1), 2144.

(10) Huang, Y. G.; Jiang, F. L.; Hong, M. C. Magnetic Lanthanide-Transition-Metal Organic-Inorganic Hybrid Materials: From Discrete Clusters to Extended Frameworks. *Coord. Chem. Rev.* **2009**, *253* (23−24), 2814−2834.

(11) Piquer, L. R.; Sañudo, E. C. Heterometallic 3d−4f Single-Molecule Magnets. *Dalton Trans.* **2015**, *44*, 8771−8780.

(12) Darago, L. E.; Boshart, M. D.; Nguyen, B. D.; Perlt, E.; Ziller, J. W.; Lukens, W. W.; Furche, F.; Evans, W. J.; Long, J. R. Strong Ferromagnetic Exchange Coupling and Single-Molecule Magnetism in MoS_4^{3-}-Bridged Dilanthanide Complexes. *J. Am. Chem. Soc.* **2021**, *143* (22), 8465−8475.
(13) Andruh, M.; Ramade, I.; Codjovi, E.; Guillou, O.; Kahn, O.; Trombe, J. C. Crystal Structure and Magnetic Properties of $[Ln_2Cu_4]$ Hexanuclear Clusters (Where Ln = Trivalent Lanthanide). Mechanism of the Gadolinium(III)-Copper(II) Magnetic Interaction. *J. Am. Chem. Soc.* **1993**, *115* (5), 1822−1829.
(14) Zhang, P.; Luo, Q.; Zhu, Z.; He, W.; Song, N.; Lv, J.; Wang, X.; Zhai, Q.; Zheng, Y.; Tang, J. Radical-Bridged Heterometallic Single-Molecule Magnets Incorporating Four Lanthanoceniums. *Angew. Chem., Int. Ed.* **2023**, *62* (12), No. e202218540.
(15) Letko, C. S.; Panetier, J. A.; Head-Gordon, M.; Tilley, T. D. Mechanism of the Electrocatalytic Reduction of Protons with Diaryldithiolene Cobalt Complexes. *J. Am. Chem. Soc.* **2014**, *136* (26), 9364−9376.
(16) Demir, S.; Zadrozny, J. M.; Nippe, M.; Long, J. R. Exchange Coupling and Magnetic Blocking in Bipyrimidyl Radical-Bridged Dilanthanide Complexes. *J. Am. Chem. Soc.* **2012**, *134* (45), 18546−18549.
(17) Evans, W. J.; Davis, B. L.; Champagne, T. M.; Ziller, J. W. C-H Bond Activation through Steric Crowding of Normally Inert Ligands in the Sterically Crowded Gadolinium and Yttrium (C_5Me_5) 3M Complexes. *Proc. Natl. Acad. Sci. U. S. A.* **2006**, *103* (34), 12678−12683.
(18) Gould, C. A.; Darago, L. E.; Gonzalez, M. I.; Demir, S.; Long, J. R. A Trinuclear Radical-Bridged Lanthanide Single-Molecule Magnet. *Angew. Chem. - Int. Ed.* **2017**, *56* (34), 10103−10107.
(19) Mrkvová, K.; Kameníček, J.; Šindelář, Z.; Kvítek, L.; Mrozinski, J.; Nahorska, M.; Žák, Z. Synthesis, Properties and Crystal Structures of $R[M^{III}(Bdt)_2]$ Complexes (M = Ni, Co, Cu). *Transit. Met. Chem.* **2004**, *29* (3), 238−244.
(20) Kubelka, P. New Contributions to the Optics of Intensely Light-Scattering Materials. *Part I. JOSA* **1948**, *38* (5), 448−457.
(21) Lim, B. S.; Fomitchev, D. V.; Holm, R. H. Nickel Dithiolenes Revisited: Structures and Electron Distribution from Density Functional Theory for the Three-Member Electron-Transfer Series $[Ni(S_2C_2Me_2)_2]^{0,1-,2-}$. *Inorg. Chem.* **2001**, *40* (17), 4257−4262.
(22) Vlček, A.; Vlček, A. A. Bis(Maleonitriledithiolato)Cobalt Redox Series. *Inorg. Chim. Acta* **1982**, *64*, L273−L274.
(23) Selby-Karney, T.; Grossie, D. A.; Arumugam, K.; Wright, E.; Chandrasekaran, P. Structural and Spectroscopic Characterization of Five Coordinate Iron and Cobalt Bis(Dithiolene)-Trimethylphosphine Complexes. *J. Mol. Struct.* **2017**, *1141*, 477−483.
(24) Miessler, G. L.; Fischer, P. J.; Tarr, D. A. *Inorganic Chemistry*; Prentice Hall: Upper Saddle River, NJ, USA, 2013.
(25) Sandman, D. J.; Allen, G. W.; Acampora, L. A.; Stark, J. C.; Jansen, S.; Jones, M. T.; Ashwell, G. J.; Foxman, B. M. Nickel, Cobalt, and Copper Complexes of o-Benzenediselenolate: Synthesis and Structural and Magnetic Properties. *Inorg. Chem.* **1987**, *26* (11), 1664−1669.
(26) Hitchman, M. A. Electronic Structure of Low-Spin Cobalt(II) Schiff Base Complexes. *Inorg. Chem.* **1977**, *16* (8), 1985−1993.
(27) Chilton, N. F.; Anderson, R. P.; Turner, L. D.; Soncini, A.; Murray, K. S. PHI: A Powerful New Program for the Analysis of Anisotropic Monomeric and Exchange-Coupled Polynuclear d- and f-Block Complexes. *J. Comput. Chem.* **2013**, *34* (13), 1164−1175.
(28) Akine, S.; Matsumoto, T.; Taniguchi, T.; Nabeshima, T. Synthesis, Structures, and Magnetic Properties of Tri- and Dinuclear Copper(II)−Gadolinium(III) Complexes of Linear Oligooxime Ligands. *Inorg. Chem.* **2005**, *44* (9), 3270−3274.
(29) Shimada, T.; Okazawa, A.; Kojima, N.; Yoshii, S.; Nojiri, H.; Ishida, T. Ferromagnetic Exchange Couplings Showing a Chemical Trend in Cu−Ln−Cu Complexes (Ln = Gd, Tb, Dy, Ho, Er). *Inorg. Chem.* **2011**, *50* (21), 10555−10557.
(30) Fellah, F. Z. C.; Costes, J.-P.; Dahan, F.; Duhayon, C.; Novitchi, G.; Tuchagues, J.-P.; Vendier, L. Di- and Triheteronuclear Cu−Gd and Cu−Gd−Cu Complexes with Dissymmetric Double Bridge. *Inorg. Chem.* **2008**, *47* (14), 6444−6451.
(31) Paulovič, J.; Cimpoesu, F.; Ferbinteanu, M.; Hirao, K. Mechanism of Ferromagnetic Coupling in Copper(II)-Gadolinium(III) Complexes. *J. Am. Chem. Soc.* **2004**, *126* (10), 3321−3331.
(32) Wang, X.; Hale, A. R.; Hill, S.; Christou, G. High-Field EPR Investigation and Detailed Modeling of the Magnetoanisotropy Tensor of an Unusual Mixed-Valent $Mn_2^{IV}Mn_2^{III}Mn^{II}$ Cluster. *Appl. Magn. Reson.* **2023**, *54* (1), 77−91.
(33) Reta, D.; Chilton, N. F. Uncertainty Estimates for Magnetic Relaxation Times and Magnetic Relaxation Parameters. *Phys. Chem. Chem. Phys.* **2019**, *21* (42), 23567−23575.
(34) Ho, L. T. A.; Chibotaru, L. F. Intermolecular Mechanism for Multiple Maxima in Molecular Dynamic Susceptibility. *Phys. Rev. B* **2018**, *98* (17), No. 174418.
(35) Blackmore, W. J. A.; Gransbury, G. K.; Evans, P.; Kragskow, J. G. C.; Mills, D. P.; Chilton, N. F. Characterisation of Magnetic Relaxation on Extremely Long Timescales. *Phys. Chem. Chem. Phys.* **2023**, *25* (25), 16735−16744.
(36) Liddle, S. T.; Slageren, J. V. Improving f-Element Single Molecule Magnets. *Chem. Soc. Rev.* **2015**, *44* (19), 6655−6669.

https://doi.org/10.1021/acs.inorgchem.4c03828
Inorg. Chem. 2024, 63, 24150−24156